Published by Avanti Publishers

International Journal of Petroleum Technology

ISSN (online): 2409-787X

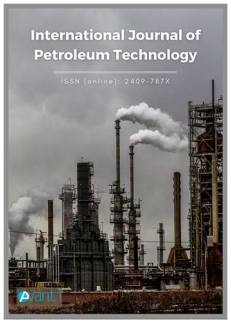

The Joint Application of Diagenetic, Petrophysical and Geomechanical Data for Selecting Hydraulic Fracturing Candidate Zone: A Case Study from a Carbonate Reservoir in Iran

E. Bakhshi[1,2], A. Shahrabadi[1,*], N. Golsanami[2,*], Sh. Seyedsajadi[3], X. Liu[4] and Z. Wang[5]

[1]*Research Institute of Petroleum Industry (RIPI), Tehran, Iran.*

[2]*College of Energy and Mining Engineering, Shandong University of Science and Technology, Qingdao, China.*

[3]*Arvandan Oil & Gas Company, Khoramshahr, Iran.*

[4]*Peking University, Beijing, China.*

[5]*China National Offshore Oil Corporation (CNOOC), Tianjin Branch.*

ARTICLE INFO

Article Type: Research Article

Keywords:
Diagenesis
Petrophysical Properties
Mechanical Earth Model
Candidate Zone Selection
Geomechanical Properties

Timeline:
Received: August 02, 2021
Accepted: September 07, 2021
Published: October 12, 2021

Citation: Bakhshi E, Shahrabadi A, Golsanami N, Seyedsajadi S, Liu X, Wang Z. The Joint Application of Diagenetic, Petrophysical and Geomechanical Data for Selecting Hydraulic Fracturing Candidate Zone: A Case Study from a Carbonate Reservoir in Iran. Int J Petrol Technol. 2021; 8: 55-79.

DOI: https://doi.org/10.15377/2409-787X.2021.08.5

ABSTRACT

The more comprehensive information on the reservoir properties will help to better plan drilling and design production. Herein, diagenetic processes and geomechanical properties are notable parameters that determine reservoir quality. Recognizing the geomechanical properties of the reservoir as well as building a mechanical earth model play a strong role in the hydrocarbon reservoir life cycle and are key factors in analyzing wellbore instability, drilling operation optimization, and hydraulic fracturing designing operation. Therefore, the present study focuses on selecting the candidate zone for hydraulic fracturing through a novel approach that simultaneously considers the diagenetic, petrophysical, and geomechanical properties. The diagenetic processes were analyzed to determine the porosity types in the reservoir. After that, based on the laboratory test results for estimating reservoir petrophysical parameters, the zones with suitable reservoir properties were selected. Moreover, based on the reservoir geomechanical parameters and the constructed mechanical earth model, the best zones were selected for hydraulic fracturing operation in one of the Iranian fractured carbonate reservoirs. Finally, a new empirical equation for estimating pore pressure in nine zones of the studied well was developed. This equation provides a more precise estimation of stress profiles and thus leads to more accurate decision-making for candidate zone selection. Based on the results, vuggy porosity was the best porosity type, and zones C2, E2 and G2, having suitable values of porosity, permeability, and water saturation, showed good reservoir properties. Therefore, zone E2 and G2 were chosen as the candidate for hydraulic fracturing simulation based on their E (Young's modulus) and ν (Poisson's ratio) values. Based on the mechanical earth model and changes in the acoustic data versus depth, a new equation is introduced for calculating the pore pressure in the studied reservoir. According to the new equation, the dominant stress regime in the whole well, especially in the candidate zones, is SigHmax>SigV>Sighmin, while according to the pore pressure equation presented in the literature, the dominant stress regime in the studied well turns out to be SigHmax>Sighmin>SigV.

**Corresponding Authors*
Emails: [1]shahrabadia@ripi.ir, abbas.shahrabadi@gmail.com, [2]golsanami_naser@sdust.edu.cn, golsanami_naser@yahoo.com
Tel: [1]+98-2148252051, [2]+86-13589295914

1. Introduction

Conservation of hydrocarbon reservoirs requires studying the reservoir's production behavior over time. Careful assessment of reservoir characteristics and studying the behavior of similar cases around the world, designing the mathematical reservoir models to achieve the optimal production plan, and using models to predict reservoir performance relative to the production process over time are the necessary factors for designing appropriate methods to improve the recovery factor. Controlling reservoir quality is one of the most important stages in reservoir evaluation. It seems that diagenesis is the main key in controlling reservoir quality development [1]. Diagenetic phenomena like cementation, dolomitization, and dissolution might lead to the formation of plenty of rock types with different properties. Hence, investigating diagenetic processes will be critical for improving the knowledge of quality controlling factors in carbonate reservoirs. Because of the complex structure of carbonate rocks that is inherited from the depositional and diagenetic processes, these rocks mostly display very heterogeneous and oblique pore networks when compared to the granular rocks [2, 3]. Generally, the most important factors influencing the diagenesis process can be divided into two main classes [4], which are sedimentary and environmental factors, as explained in detail in Figure **1**.

Petrophysical properties have the main role in reservoir evaluation. By estimating the fluid types and their volume as well as the rock and mineral types, petrophysical studies will help to provide comprehensive information about the reservoir. Therefore, in various types of research studies, including reservoir characterization [5-13], hydraulic fracturing simulation/operation [14-23], and building, evaluating, and controlling numerical models [24, 25], petrophysical parameters play a vital role. Porosity, permeability, and water saturation, which are considered as three main reservoir petrophysical properties, are provided by core or well-logging data.

Geomechanical studies are very critical in the whole hydraulic fracturing process, especially in unconventional reservoirs. Drilling, wellbore stability, and hydraulic fracturing operations are greatly affected by the geomechanical properties of the reservoir. Therefore, building a mechanical earth model (MEM) is very useful for demonstrating the geomechanical behavior of the subsurface mathematically. A MEM numerically displays the mechanical rock properties, stresses, and pore pressure that act at different depths [26]. Many researchers around the world have developed the MEM for determining the reservoir mechanical properties [27-31], hydraulic fracturing purposes [32-35], or wellbore instability analysis [36-38]. Constructing the mechanical earth model is an input for such other studies as wellbore stability, hydraulic fracturing, and predicting the mud weight window (MWW) [39]. A mechanical earth model describes the reservoir's mechanical parameters such as rock strength, elastic properties, the state of in situ stresses, and pore pressure. Kidambi *et al*. [40] constructed a 1D MEM for a vertical well in a naturally fractured tight carbonate gas reservoir in the Persian Gulf and investigated the wellbore stability, rock deformation, and regional stress trends. They also designed a safe mud weight window (SMWW) for the wellbore. Zain *et al*. [41] used the log data and, by calculating elastic properties and building a 1D MEM, estimated the vertical and horizontal stresses at well locations at the Molasse Basin in southern Germany. Heydarabadi *et al*. [42] studied the candidate well selection procedure for hydraulic fracturing operations. They concluded that the reservoir permeability, in-situ stress profiles, and existing natural fractures are the most important parameters in selecting candidate wells in hydraulic fracturing treatments.

The complete knowledge of the reservoir would lead to more accurate and complete designs and planning. Diagenetic processes as well as petrophysical and geomechanical properties, especially in carbonate reservoirs, are interconnected as the links in a chain, and combining them could definitely provide a more precise and comprehensive understanding of the reservoir. Therefore, by conducting more preliminary studies, the probability of designing and succeeding in hydraulic fracturing operations and selecting the suitable candidate zones for this purpose will be increased. Numerous studies have been conducted for planning hydraulic fracturing operations and selecting candidate wells/zones in the world's oil reservoirs, especially in Iranian carbonate reservoirs [43-47]. However, despite the significant impact of diagenesis, petrophysical and geomechanical properties, no study has comprehensively considered these three procedures and their relationships for a more accurate selection of hydro-fracturing candidate zone. Thus, in this study, we decided to address the shortcomings of the previous studies. For this purpose, the joint application of diagenetic, petrophysical, and geomechanical data was used for selecting hydraulic fracturing candidate zones.

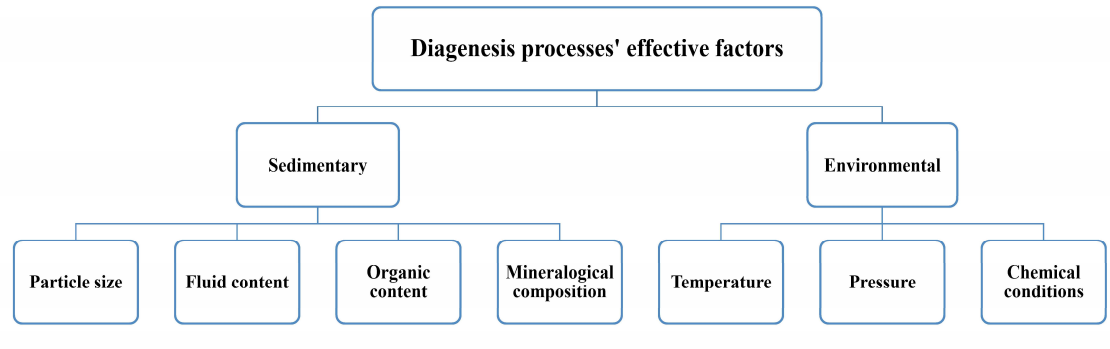

Figure 1: The most important factors that influence the course of diagenesis.

The primary purpose of the present study is to select the candidate zone for hydraulic fracturing operation in one of the oil fields in central Iran. The study was carried out using a subject well, Well#A, suggested by the engineers of the National Iranian South Oil Company (N.I.S.O.C) and was divided into three main phases, which included selecting the zones with a good reservoir quality, obtaining the geomechanical parameters, and developing the mechanical earth model. As for the first phase and for determining the porosity types, the diagenetic processes in the selected well were studied, and based on the conducted laboratory test results (see section 3.1), the main diagenetic processes that have occurred in the studied well were analyzed thoroughly; and the diagenesis features were estimated. Thus, the main petrophysical parameters, including porosity, permeability, and water saturation, were determined in the studied well. As a result, three zones, including C2, E2, and G2, were selected as potential candidates for hydraulic fracturing simulation. In the second phase, the full-set petrophysical well logs were provided, and the geomechanical parameters of this well were determined using empirical relationships. These geomechanical parameters included elastic properties, i.e., Young's modulus (static and dynamic), Bulk modulus (static and dynamic), Shear modulus (static and dynamic), and Poisson's ratio, as well as the strength parameters, i.e., unconfined compressive strength (UCS), tensile strength (T), and friction angle (FANG) and also principal stresses and pore pressure. It is worth noting that estimating reservoir geomechanical parameters are fundamental in various areas, from constructing the MEM to simulating hydraulic fracturing in the reservoir and in studying the reservoir compaction and subsequent surface subsidence caused by previous operations. Finally, the one-dimensional mechanical earth model of our subject well was constructed, and based on the results of the preceding two phases, the candidate zones for hydraulic fracturing operation were selected. It is worth noting that the innovation of this study lies in the fact that because of the variable structures and characteristics of rocks at different depths and formations, in this study, for the first time, an empirical relation for calculating pore pressure in different zones of the studied well was obtained. This relation provides more acceptable results for calculating the stress profiles. The three phases of the current study are summarized in Figure **2**.

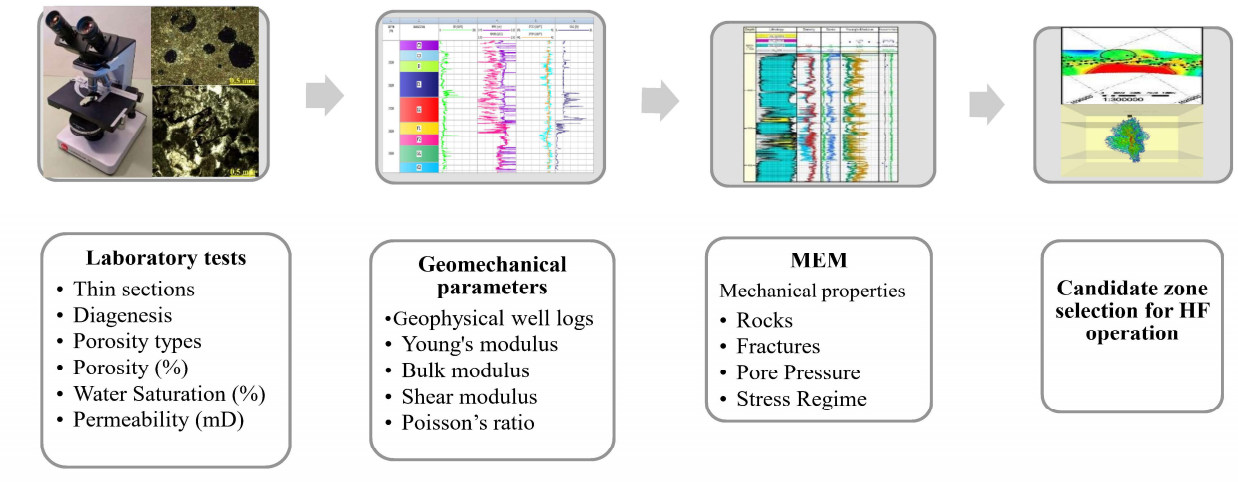

Figure 2: Flow chart showing in the main research steps of this study.

2. Geological Setting and Stratigraphy of the Study Area

The studied oil field is close to the Ahvaz city in the south of Iran, in the southern boundary of Dezful Embayment, and the northeast of the Arabian Plate (Figure **3**). The studied reservoir (Bangestan group) includes carbonate rocks of Ilam, Sarvak, and Kazhdumi formations that were discovered in 1959 on the Ilam formation. To the time being, more than 72 production fields have been discovered from the Bangestan group in southwestern Iran, where Ilam and Sarvak are two of the most productive reservoirs of this group. The largest oil accumulations in Bangestan group reservoirs is more than 10 billion barrels, but despite the large volumes of initial crude oil in place, the recovery factors of the reservoir are not high enough (between 20 to 30%) [48]. Therefore, it can be said that this reservoir might be a suitable option for performing hydraulic fracturing operations. In Figure **4**, the stratigraphy of the Ilam and Sarvak formations is presented. Also, due to the similarity of the studied area to the S-SE stratigraphy of Iraq, the Cretaceous stratigraphy in parts of the Persian Gulf is shown in Figure **4**. Based on the previous studies, it can be said that diagenesis has played an important role in the development of the Sarvak Formation in the reservoir. Esrafili-Dizaji *et al*. [49, 50] believed that during a phase of mid-Cretaceous uplift, the dissolution porosity was developed, so the top of the Sarvak Formation became subaerially exposed, leached, and fractured.

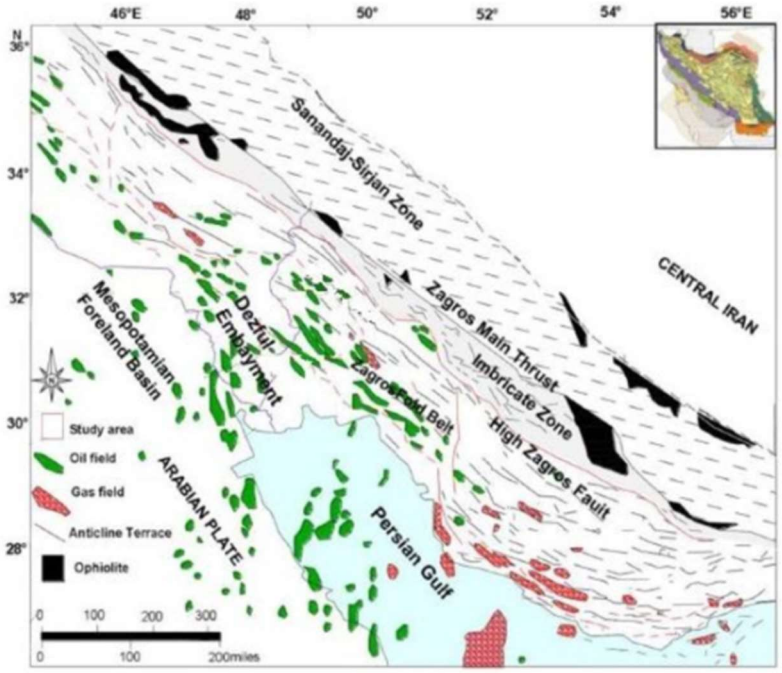

Figure 3: Tectonic map of the study area (Modified after [51]).

Based on the studies' results, the average porosity and permeability of the Sarvak formation are about 13% (varies between 5-25%) and 14 mD, respectively. The Sarvak carbonates are thick with rudist-dominated intervals that have good potential for reservoir development. The thickness of the Ilam Formation is very changeable, and it mostly consists of mud-dominated deposits with occasional grain-dominated intervals. Furthermore, based on the existing literature, the average porosity of Illam formation is larger than 10%, while the mean permeability is smaller than 10 mD. Bordenave *et al*. [52] explained that the Albian Kazhdumi formation (see Figure **4**) is the principal source of the hydrocarbons in the Sarvak and Ilam reservoirs. Hence, it should be noted that due to changes in the facies trend of the Sarvak and Ilam formations, they were divided into different zones. In the preliminary studies of the Bangestan reservoir, the reservoir was divided into ten zones. However, over time, this zonation was modified due to changes in the facies. Based on the latest zonation done by the National Iranian South Oil Company experts, the Ilam formation is divided into five zones (A to C3), and the Sarvak formation is divided into 12 units (D to J).

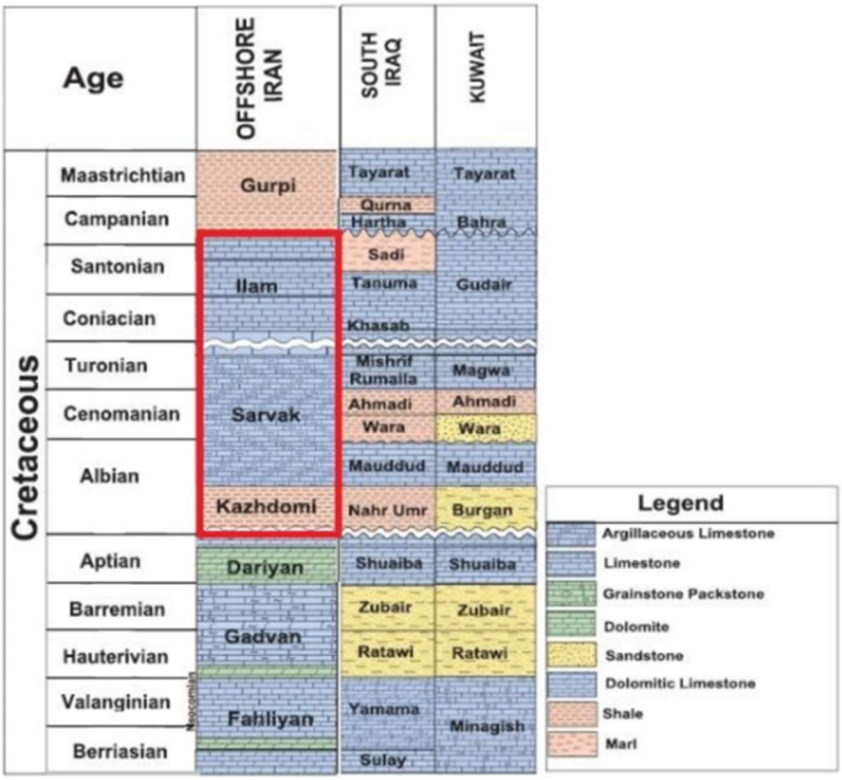

Figure 4: Sequence stratigraphy section of formations from SW of Iran to SE of Iraq (Modified after [51].

2.1. Stratigraphic Studies of Well#A

The Illam and Sarvak Formations in Well#A are mainly composed of limestone in cream to white and sometimes light brown colors. Besides, the thickness of these formations in this well is 166.5 (m) and 764 (m), respectively. As mentioned in the previous section, the Illam and Sarvak formations are divided into different zones. However, since our study results included selecting the candidate zones of C2, E2, and G2, only the petrophysical properties of these zones are described in this section as follows: (i) **Zone C2** consists of Packstone-Wackestone, which is formed by reducing the clay volume and the entrance of Rudist debris in high-energy conditions. The average thickness of this zone is 46 meters with a porosity of 14.5% and water saturation of 21%, and an average net to gross thickness (Net/Gross) of .0.4, which shows good reservoir properties. (ii) **Zone E2** is made of Greenstone to Packstone with good porosity, which includes the best reservoir parameters in terms of the reservoir rock. The average thickness of this zone is about 80 (m) and varies from a minimum of 60 (m) to a maximum of 125 (m). The average porosity of this zone is 8%, and the average water saturation (S_w) in this zone is about 35%. With an average net to gross thickness (Net/Gross) of 0.9, this zone shows good reservoir properties; (iii) **Zone G2** mainly includes Greenstone. The average thickness of this zone is 60 (m), and its average porosity is 10%, which reaches a maximum of 20%. The average water saturation (S_w) and the ratio of net to gross thickness are 37% and 0.34, respectively.

3. Materials and Methods

Two sets of data were used for this study, including (a) core samples and thin sections for investigating the physical and petrophysical properties and diagenetic process of the reservoir, which were provided by N.I.S.O.C, and (b) geophysical well logs for determining geomechanical parameters. For estimating reservoir petrophysical properties, i.e., porosity, permeability, and water saturation, 176 core samples were selected from 4 neighboring boreholes, and the results of the tests are represented in Table **3**. Water saturation was measured directly in plug samples drilled (with oil lubricant) regularly through a cored interval using the Dean & Stark technique. Porosity was measured using helium expansion and the application of Boyl's Law to quantify grain volume or pore volume.

Also, to study the diagenetic processes (dissolution, cementation, compaction, and dolomitization) as well as porosity types (based on Choquette & Pray classification [53]), 120 core samples were acquired from 4 boreholes, and the thin sections were analyzed under a polarizing microscope. Image analysis by polarizing microscope based on rock sections offers the possibility of pore identification, grain segmentation, and mineral classification.

Figure **8** shows the porosity types and diagenetic processes based on the thin section analysis for Well#A. The well logs, including gamma-ray, neutron, and density logs, were used to draw the lithological columns (see Figure **8**).

3.1. Studied Diagenetic Processes

The role of diagenetic processes in carbonates porosity development is very important, especially in marine, meteoric, and burial environments [54]. Generally, these processes can have positive or negative effects on the reservoir. For instance, processes such as dissolution and dolomitization increase the porosity, permeability, and, therefore, the reservoir quality. While, in many other cases, diagenetic processes like cementation can reduce the porosity and permeability [55] and consequently lead to loss of the reservoir quality. Hence, recognizing the main diagenetic processes plays an important role in understanding the changes in reservoir quality. The main diagenetic processes that have occurred in the studied wells are as follows:

- **Dissolution:** Dissolution is one of the main diagenetic processes that mainly causes secondary porosity such as moldic, vuggy, and channel porosity. Dissolution takes place in meteoric, marine, and burial environments. In Figure **6a**, the microscopic images of dissolution are shown.

- **Cementation:** Cementation is the main diagenetic process and includes all the processes that cause the minerals to settle in the primary or secondary cavities in the rock. In definition, cement is the chemical substance that deposits from the supersaturated solutions contained in the rock cavities [56]. High-magnesium calcite (HMC), low-magnesium calcite (LMC), aragonite, and dolomite are the most common carbonate types of cement in limestone, while anchorite, siderite, kaolinite, quartz, anhydrite, gypsum, and halite are less common [57]. In Figure **6b**, the microscopic images of cementation are shown.

- **Compaction:** Compaction is a burial diagenesis process that is observed in the following forms:

  Mechanical Compaction: Can begin immediately after deposition.

  Chemical Compaction: Usually occurs at depths of more than a few hundred meters.

  The initial sediment composition, especially the amount of limestone and clay, and the initial diagenetic history, especially the cementation degree, are of great importance in how the compaction is formed [58].

  In this study, the results of chemical compaction are mainly considered, and the process of their changes along the studied sections is investigated. Dissolution seams and Stylolite are the two main phenomena of chemical condensation. In Figure **6c**, the microscopic images of the compaction phenomenon are shown.

- **Dolomitization:** During the contact between limestone and magnesium-rich water, dolomite, calcium, and magnesium carbonate, replace the calcite in the rock. This process is named dolomitization. Dolomitization enables the carbonate reservoir to withstand compaction. In general, in shallow areas, dolomites have less porosity than limestone, but dolomites retain their porosity better during the burial process. Recrystallization on a large scale happens during the dolomitization [59]. In Figure **6d**, the microscopic images of dolomitization are shown.

3.1.1. Porosity Types

The best way to identify different types of porosity is to study thin sections with a polarizing microscope, which was implemented in this study. The main types of porosity by calculating their percentage along the studied sections are described as follows, and the results are shown in Figures **7** and **8**.

- **Moldic porosity:** It is a type of secondary porosity created through the dissolution of a preexisting constituent of a rock. Selective dissolution in Aragonite grains of limestone creates empty spaces in the location of these grains, which are quite similar to the original grain [60]. The pore space preserves the shape or mold of the dissolved material. This porosity is selected by the rock fabric and is secondary (usually during atmospheric and burial diagenesis) [61]. Microscopic images of mold porosity are shown in Figure **7a**, and its variations along the sections studied are shown in Figure **8**.

- **Intraparticle porosity:** Intraparticle depositional porosity constitutes one of the fundamental differences between carbonate and siliciclastic porosity and may originate in various ways. This porosity is less important in terms of oil storage among all types of porosity in carbonate rocks, especially if it is closed and unused because the cavities within the grain may not be interconnected [62]. Microscopic images of intraparticle porosity are shown in Figure **7b**, and its variations along the studied sections are shown in Figure **8**.

- **Interparticle porosity:** The grain porosity is not mainly preserved in the carbonate rocks because these rocks are very sensitive to compaction, and this kind of porosity which is a type of primary porosity after burial, will disappear immediately. Also, cementing process during the burial process has a destructive role in maintaining the interparticle porosity. In this study, the percentage of this porosity is shown along the studied sections. Microscopic images of interparticle porosity are shown in Figure **7c**, and its variations along the studied sections are shown in Figure **8**.

- **Vuggy porosity:** Dissolution of some part of the rock will cause creating cavities that may sometimes cut the fabric of the rock. This kind of porosity may initially be such as mold porosity for which the original shape has changed and expanded due to dissolution [63]. The most common porosity in the studied sections of this study was vuggy porosity. Microscopic images of the vuggy porosity are shown in Figure **7d**, and its changes along the studied sections are shown in Figure **8**.

- **Microfracture porosity:** Collapse, dissolution, slump, and tectonic forces within the sediments and calcareous layers are the main reasons causing this kind of porosity. By increasing the dissolution process in the sediments, this porosity becomes shear porosity [56]. Microfracture porosity in carbonate rocks is very common and mostly occurs after the burial of sediments. Microfracture porosity has a high frequency in the studied sections along with vuggy porosity. Microscopic images of microfracture porosity are shown in Figure **7e**, and its changes along the studied sections are shown in Figure **8**.

3.2. Determining Geomechanical Parameters by Using Petrophysical Well Logs

This research study employed Well#A, a vertical exploration well drilled till 3980 m TVD (true vertical depth) in one of the Iranian southwest oil fields. Wireline logs (Gamma Ray, Caliper, Sonic, Density, and Neutron) and extended leak-off test (XLOT) measurements were available in this well. Figure **5** shows the input logs used for determining geomechanical parameters and also constructing the MEM in this study. In this figure, from the left, the first track shows the depth in meters. The second track shows the formation tops. Track 3 includes the GR. Track 4 shows porosity and density. In track 5, compression and shear profiles are shown; and in track 6, the caliper log is shown.

Considering the available data sets, different methods might be used for estimating the geomechanical parameters such as experimental studies [64], empirical correlations [65], using well logs [66, 67], etc. The fundamental of these methodologies is the relationship between the rock physical and mechanical properties, such as the relationship between the elastic wave velocity with density curves in petrophysical logs or the relationship between the elastic wave velocity and mechanical properties like uniaxial compressive strength.

3.2.1. Elastic Properties

Estimating the uniaxial compressive strength (UCS) and rock elastic properties (Young's modulus, Poisson's ratio) are essential for determining principal stresses ($\sigma_H, \sigma_h, \sigma_v$), wellbore instability analysis, designing hydraulic fracturing, and predicting optimum mud pressure. Consequently, in this study, based on the available well-logging data, we used a log-based method to determine rock elastic properties and obtain the magnitude of principal stresses.

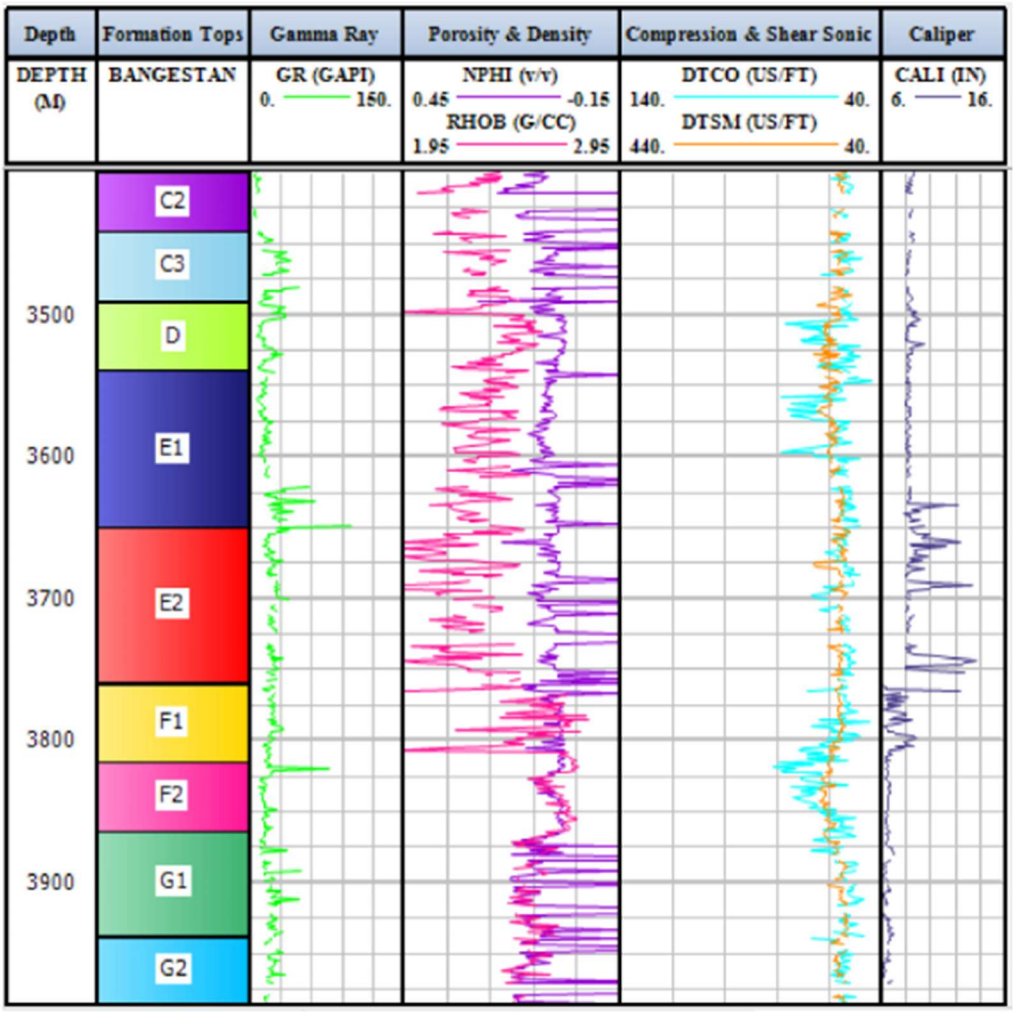

Figure 5: The petrophysical input logs used for construction of MEM in Well#A.

- **Young's modulus (E):** Dynamic Young's modulus (E_{dyn}) (Pa) is estimated based on Equation (1). In Equation .1, E_{dyn} is in relation with the rock density (ρ) (kg/m^3), compression (V_p) (m/s), and shear wave velocity (V_s) (m/s) (V_p and V_s could be calculated by reversing the compressional wave delay time (DTCO) and shear wave delay time (DTSM) from the sonic log) [68].

$$E_{dyn} = \frac{\rho V_s^2 (3V_p^2 - 4V_s^2)}{V_p^2 - V_s^2} \quad (1)$$

Based on the empirical relation suggested by the researchers of National Iranian South Oil Company (N.I.S.O.C), the static Young's modulus (E_{sta}) was estimated as in Equation (2).

$$E_{sta} = 0.7 E_{dyn} \quad (2)$$

- **Poisson's ratio (ν):** Estimation of dynamic Poisson's ratio could be done by using Equation (3). It should be mentioned that the dynamic parameters are calculated based on the well-logging data, and for converting them to the static parameters, some empirical relations are proposed. In this study, these relations are proposed by N.I.S.O.C as also used in the previous section. Accordingly, the dynamic Poisson's ratio (ν_{dyn}) was equal to the static Poisson's ratio in this study (Equation. 4).

$$\upsilon_{dyn} = \frac{V_p^2 - 2V_s^2}{2(\mathrm{V}_p^2 - \mathrm{V}_s^2)} \tag{3}$$

$$\nu_{sta} = \nu_{dyn} \tag{4}$$

- **Shear modulus (G):** The Shear modulus is used to explain the behavior of a material (rock) when it is subjected to shearing stress. Based on the common relationship between Young's modulus, Poisson's ratio, and the Shear modulus (Equation. 5), if the static Young's modulus is calculated, the static shear modulus (Pa) can be obtained according to Equation (6).

$$G = \frac{E}{2(1+\nu)} \tag{5}$$

$$G_{sta} = \frac{E_{sta}}{2(1+\nu_{sta})} \tag{6}$$

For estimating dynamic Shear modulus (Pa), Equation (7) could be used.

$$G_{dyn} = \rho V_s^2 \tag{7}$$

- **Bulk modulus (K):** Similar to the Shear modulus, the Bulk modulus is also calculated based on the three parameters, including Young's modulus, Poisson's ratio, and the Bulk modulus (Equation. 8). Hence, by inserting the static Young's modulus and Poisson's ratio values, the static Bulk modulus (K_{sta}) (Pa) is estimated (Equation. 9).

$$K = \frac{E}{3(1-2\nu)} \tag{8}$$

$$K_{sta} = \frac{E_{sta}}{3(1-2\nu_{sta})} \tag{9}$$

And the dynamic Bulk modulus (Pa) is obtained by using Equation (10).

$$K_{dyn} = \rho(V_p^2 - \frac{4}{3}V_s^2) \tag{10}$$

3.2.2. Strength Parameters

Determining rock strength parameters, especially Unconfined Compressive Strength (UCS) is very important in rock mechanical studies. However, in most cases, estimating UCS by using standard methods is time-consuming and costly, mainly due to difficult sample preparation and destructive procedure of the test or unavailable core samples. Therefore, in this study, the rock strength parameters were calculated by the log-based method explained in the following section.

- **Unconfined Compressive Strength (UCS):** Based on the availability of data, the UCS could be estimated dynamically from sonic log data-derived E_{sta}, E_{dyn}, or V_p. But according to the N.I.S.O.S researchers' suggestion, the UCS was determined by using the below empirical equation (Equation 11).

$$UCS = 2.27E_{sta} + 4.7 \tag{11}$$

- **Tensile strength (T):** The rock tensile strength varies from $\frac{UCS}{12}$ to $\frac{UCS}{8}$ depending on the formation type, where for the carbonate fractured formations, generally, the smallest value is adopted [69]. But in this study and due to the N.I.S.O.C experts' research results, the tensile strength for the limestone (dominant formation material in the studied well) was calculated by Equation (12).

$$T = 0.08UCS \tag{12}$$

- **Friction Angle (FANG):** The internal friction angle (FANG) (Degree) of rock is calculated using a common experimental relation in rock mechanics obtained by Plumb for sandstones and carbonates [70] (Equation. 13).

$$FANG = 26.5 - 37.4(1 - NPHI - V_{shale}) + 62.1(1 - NPHI - V_{shale})^2 \tag{13}$$

The variables in Equation (13) are the amount of formation porosity read by the neutron log (NPHI) as well as the shale volume. The shale volume is obtained by using the gamma-ray log (SGR) (see Equation 14).

$$V_{shale} = \frac{GR - GR_{\min}}{GR - GR_{\max}} \tag{14}$$

Where GR_{min} and GR_{max} are the minimum and maximum GR log readings, respectively. The elastic properties and strength parameters for different zones of studied Well#A are shown in Table **1** and Figure (**11**), which shows the 1D MEM.

3.2.3. Stresses

In this step, the principal stresses and pore pressure were estimated.

- **Vertical stress (σv):** The vertical stress for onshore or offshore areas based on the overburden could be obtained by Equation (15) using the bulk density log. But in the present study, the density log just ran across the reservoir section and was rarely available in the first few hundred meters of a well. In some intervals into the wellbore, no density log is available. Therefore, for estimating the density of the formations within these intervals, the density log is extrapolated to the surface (see Figure **9**).

$$\begin{aligned} Onshore \rightarrow \sigma_v &= \int_0^z \rho(z) g dz \approx \bar{\rho} g z \\ Offshore \rightarrow \sigma_v &= \rho_w g z_w + \int_{z_w}^z \rho(z) g dz \approx \rho_w g z_w + \bar{\rho} g (z - z_w) \end{aligned} \tag{15}$$

Where, σ_v is the overburden pressure (MPa), $\rho(z)$ is the bulk density of the overlying rock and fluids, and g is the gravitational acceleration (m/s^2). The average density of the sedimentary clastic rocks is 2.3 gr/cm^3. Thus, 0.023 MPa/m (1 psi/ft) is a good estimation of the overburden gradient. In offshore, the density of water is 1 gr/cm^3 (also, the gradient range is 0.43 psi/ft).

- **Pore pressure (PP):** In this study, the pore pressure was estimated by the Eaton method (Equation. 16) from sonic log data [71].

$$P_P = \sigma_v - (\sigma_v - Ph).\left(\frac{DT_n}{DT}\right)^x \quad (16)$$

Where σ_v is the overburden pressure obtained from Equation. 15, *Ph* is hydrostatic pressure (about 0.433 psi/ft or 9.792 kPa/m) [72], DT_n is the acoustic travel-time from the normal compaction trend at the investigation depth, and Δt is the observed acoustic travel-time from the sonic log. '*x*' is an Eaton exponent and generally is 3.0 for sediments in cases the overpressure is generated by disequilibrium compaction [73]. In this research, the acoustic travel-time was determined by Equation (17).

$$DT_n = 0.000234D + 50.078 \quad (17)$$

Where D is the vertical depth.

- **Horizontal stresses (σ_H, σ_h):** In this step, the maximum (σ_H) and minimum (σ_h) horizontal stresses must be estimated. Considering the poroelastic equations and such parameters as Poisson's ratio (ν), vertical stress (σ_v), horizontal strains ($\varepsilon_x, \varepsilon_y$), pore pressure ($P_P$), and Biot's coefficient (α), the horizontal stresses can be calculated from Equations. 18 and 19.

$$\sigma_H = \frac{\nu}{1-\nu}.\left(\sigma_v - \alpha.P_p\right) + \alpha.P_p + \frac{E_{sta}}{\left(1-\nu^2\right)}.\left(\varepsilon_y + \nu.\varepsilon_x\right) \quad (18)$$

$$\sigma_h = \frac{\nu}{1-\nu}.\left(\sigma_v - \alpha.P_p\right) + \alpha.P_p + \frac{E_{sta}}{\left(1-\nu^2\right)}.\left(\varepsilon_x + \nu.\varepsilon_y\right) \quad (19)$$

Also, ε_x and ε_y could be estimated by Equations. 20 and 21 [40].

$$\varepsilon_x = \frac{\sigma_v.\nu}{E}.\left(\frac{1}{1-\nu} - 1\right) \quad (20)$$

$$\varepsilon_y = \frac{\sigma_v.\nu}{E}.\left(1 - \frac{\nu^2}{1-\nu}\right) \quad (21)$$

Where ε_x and ε_y are tectonic strains corresponding to the σ_h and σ_H. The σ_h was calibrated by extended leak-off test (XLOT). In addition, the Biot's coefficient is determined based on the rock's poroelastic behavior, but in this study was considered equal to 1. The profile of stresses and pore pressure are shown in Figure **12**.

After all, the main steps adopted for constructing a mechanical earth model were:

1. Identifying the formations based on the matrix structure.
2. Determining the rock properties, including Young's modulus, Poisson's ratio, Shear and Bulk modulus, strength properties, and tensile strength.
3. Determining principal stresses, including vertical stress, as well as the minimum and maximum horizontal stresses.
4. Determining pore pressure.
5. Calibrating estimated values of stresses and pore pressure using XLOT and RFT data.

4. Results and Discussion

In carbonate rocks (limestone and dolomite), the following processes can form the secondary porosity: (a) Freshwater dissolution in various environments such as sub-unconformity meteoric, eogenetic, or telogenetic, and (b) Dissolution by chemically aggressive subsurface fluids that happens during the organic matter maturation in the source rocks, in the deep-burial (mesogenetic) environments. With this in mind, in the studied well, four main diagenetic processes, including dissolution, cementation, compaction, and dolomitization, were investigated, which are shown in Figures **6a** to **6d**, respectively.

Despite the similarity of all pore types formed in these environments, for estimating their origin, the thin-section petrography and stable carbon-oxygen isotope analysis could be done [74]. The moldic, intraparticle, interparticle, vuggy, and microfracture porosities were the main porosity types identified in this study which are described in Figures **7a** to **7e**, respectively. Due to the low porosity and especially low permeability of carbonate reservoirs of the area, such dissolution structures as pores, fractures, and karst caves will be expanded so that the heterogeneity of these formations will be stronger. Also, natural microfractures and dissolved pores are the main storage spaces and provide a large contribution to oil production. Based on our result, microfracture and vuggy porosities had a high frequency in the studied sections, which confirms the aforementioned discussion (see Figure **8**).

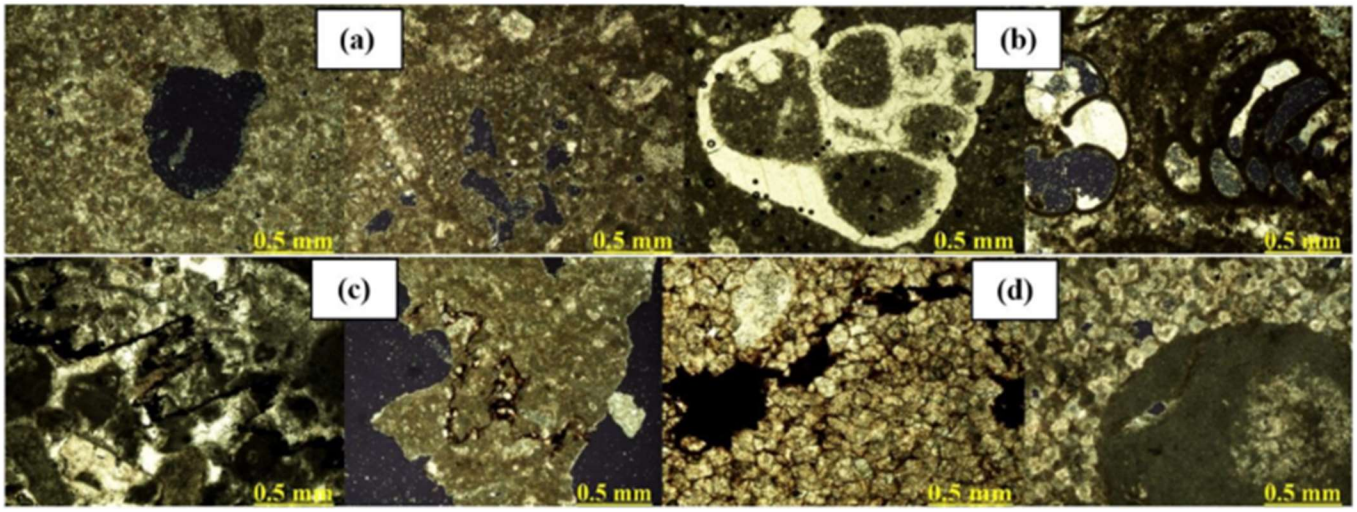

Figure 6: Microscopic images of (a) Dissolution, (b) Different fabric cements (cementation), (c) Compaction phenomenon, and (d) Dolomitization of studied well sections.

In this study, the rock elastic properties, unconfined compressive strength, friction angle, pore pressure, and principal stresses were estimated by using available well-logging data of Illam and Sarvak formations of the studied reservoir and empirical equations. Despite the great performance of some empirical equations like Archie's equation in carbonate and sandstone reservoirs [68], in some cases, empirical equations are not suitable to be used with all the data related to the rock physical and strength properties. In these cases, performing local calibration is emphasized. Accordingly, in this study, the local calibrations were done, and all the empirical equations were suggested by the N.I.S.O.C researchers. In the following, the estimated parameters for different zones are described and are represented in Tables **1** and **2**. Determining principal stresses and pore pressure is one of the main steps in constructing MEM and designing hydraulic fracturing. In this study, these parameters were estimated by using petrophysical logs data and empirical relations. Drilling reports, XLOT data points, and RFT data points were used for calibrating stresses and pore pressure. The estimation results are shown in Table **2**.

For estimating the formation density of intervals with no density log, the extrapolation of density log to the surface was conducted, and also, the density of near-surface rocks was estimated at around 1.9 gr/cm^3 (see Figure **9**). It should be noted that in this study, the density log was used to estimate the magnitude of vertical and horizontal stresses.

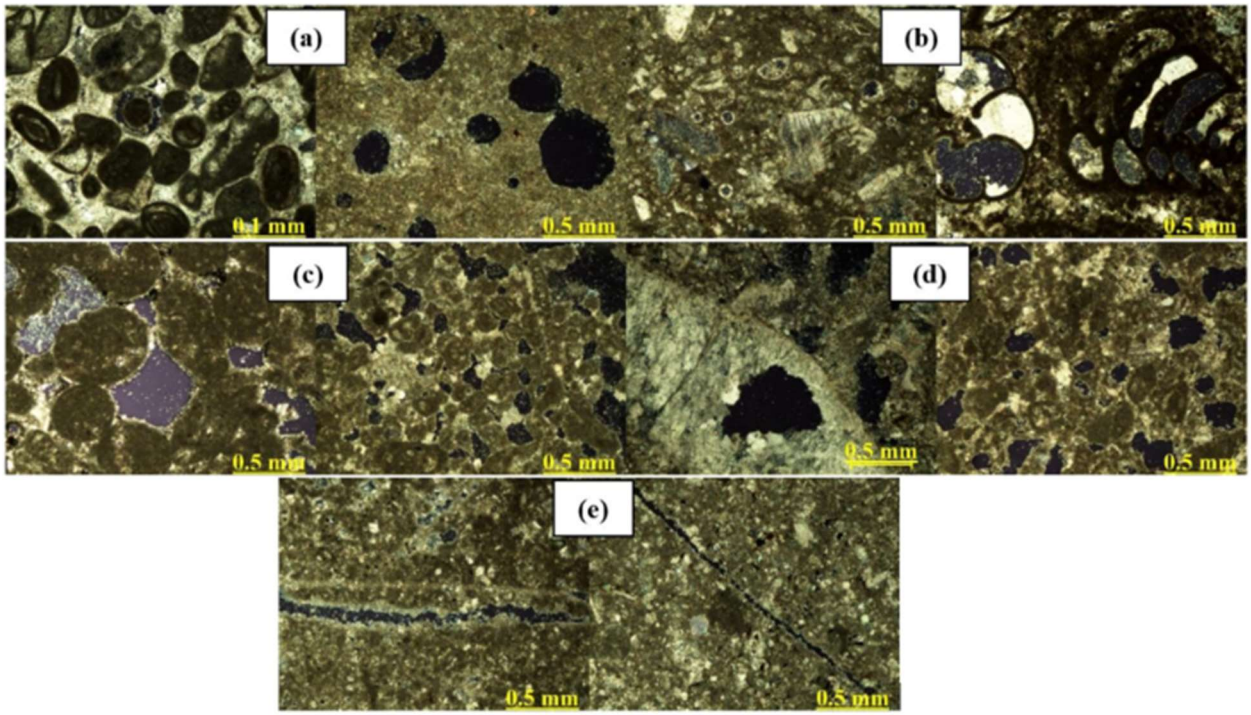

Figure 7: Microscopic images of various forms of (a) Mold porosity, (b) Intraparticle porosity, (c) Interparticle porosity, (d) Vuggy porosity, and (e) Microfracture porosity.

Table 1: Distribution of mechanical properties as well as top and bottom of formation zones in Well#A.

Zone	E_{sta} (GP)	E_{dyn} (GPa)	ν	G_{sta} (GPa)	G_{dyn} (GPa)	K_{sta} (GPa)	K_{dyn} (GPa)	UCS (MPa)	T (MPa)	FANG (DEG)
C2	35.448	50.639	0.303	13.665	19.521	31.166	44.523	85.17	6.813	42.76
C3	35.975	51.393	0.308	13.816	19.737	32.897	46.995	86.36	6.909	46.43
D	29.759	42.513	0.343	11.107	15.868	34.664	49.521	72.25	5.780	49.01
E1	31.097	44.424	0.318	11.815	16.879	30.588	43.697	75.29	6.023	46.92
E2	34.546	49.352	0.295	13.423	19.175	30.491	43.559	83.12	6.650	47.32
F1	37.241	53.202	0.297	14.372	20.532	32.948	47.069	89.24	7.139	48.53
F2	30.018	42.884	0.298	11.571	16.530	28.256	40.366	72.84	5.827	48.74
G1	40.816	58.309	0.305	15.696	22.423	36.876	52.681	97.4	7.788	43.48
G2	38.997	55.710	0.296	15.108	21.583	33.472	47.818	93.22	7.458	42.23

Table 2: Pore pressure and stress profiles in Well#A.

Parameter	Min (MPa)	Max (MPa)	Mean (MPa)
Pore Pressure	14.83	78.00	43.57
SigV	76.64	89.82	83.34
SigHmax (σ_H)	45.07	128.12	97.37
Sighmin (σ_h)	31.15	104.08	78.87

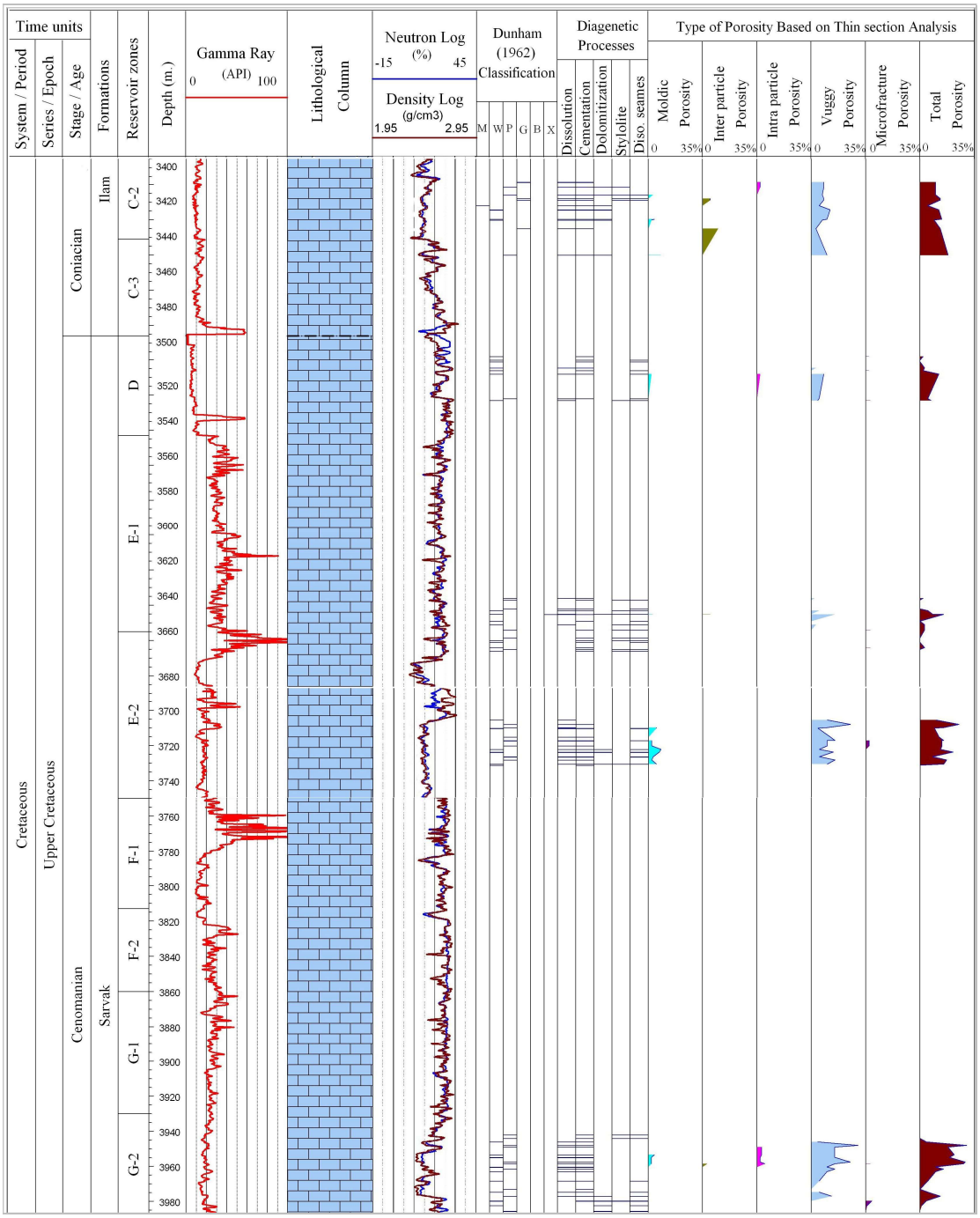

Figure 8: Distribution of diagenetic processes identified in the stratigraphic column of Ilam and Sarvak formations, Well#A.

4.1. The New Empirical Equation of Pore Pressure for the Studied Reservoir

Generally, pore pressure could be estimated based on direct or indirect methods. Direct measurements are performed by using various downhole instruments, and indirect methods are conducted by employing available geophysical logs like sonic, density, resistivity, etc. [75-77]. In well logging operations, the sonic log is the most common diagram that is usually driven from the ground to the bottom of the well along with the gamma-ray log. Therefore, in this study, the pore pressure profile was estimated by using the sonic log data (DT_n). Initially, a general equation was obtained for the whole studied depth (Equation. 22).

$$DT_n = 0.000317D + 53.08 \quad (22)$$

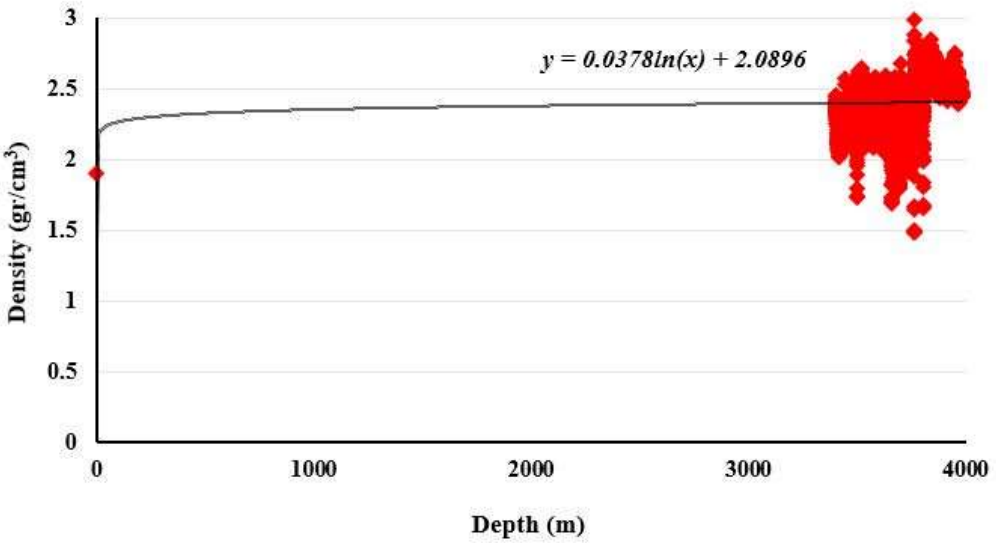

Figure 9: Density extrapolation to the surface for intervals with no density log.

Where DT_n is the acoustic travel-time from the normal compaction trend at the investigation depth and D is the vertical depth.

In the next step, the pore pressure was calculated based on the depth and sonic log (DT_n) for each of the nine studied zones (Equations. 23 to 31).

Zone

C2 $$DT_n = 0.01890D - 157.1 \quad (23)$$

C3 $$DT_n = -0.00063D + 61.1 \quad (24)$$

D $$DT_n = -0.01207D + 196 \quad (25)$$

E1 $$DT_n = -0.01997D + 293.5 \quad (26)$$

E2 $$DT_n = -0.00676D + 137.3 \quad (27)$$

F1 $$DT_n = 0.04198D - 464.9 \quad (28)$$

F2 $$DT_n = -0.12339D + 1619.4 \quad (29)$$

G1 $$DT_n = -0.02239D + 340.6 \quad (30)$$

G2 $$DT_n = -0.01507D + 251.4 \quad (31)$$

Based on Equation.22, pore pressure and stress profiles in Well#A were plotted, and also the statistical parameters were determined, which are displayed in Table **3** and Figure **12b**, respectively.

Table 3: Pore pressure and stress profiles in Well#A (Based on the introduced empirical equation).

Parameter	Min (MPa)	Max (MPa)	Mean (MPa)
Pore Pressure	3.9	78.97	33.83
SigV	76.64	89.82	83.34
SigHmax (σ_H)	45.67	138.37	97.47
Sighmin (σ_h)	26.11	118.33	77.65

4.2. Mechanical Earth Model (MEM) for Well#A

As described in the previous section, the elastic rock properties, UCS, and principal stresses were determined by using different equations and wireline logs. Accordingly, the mechanical earth model of the reservoir was constructed as follows. The mechanical earth model is the comprehensive collection of measured data and models which demonstrate the mechanical rock properties, fractures, stresses, pressures, and temperatures that act at different depths. In Figure **10**, the required data set for building a mechanical earth model are listed. As shown in Figure **10**, the essential parameters like principal stresses, fluid pressure, elastic parameters, etc. are required for geomechanical analysis and constructing mechanical earth models. This database may be obtained from a wide range of data, including seismic data, drilling data, log data, field measurements, etc.

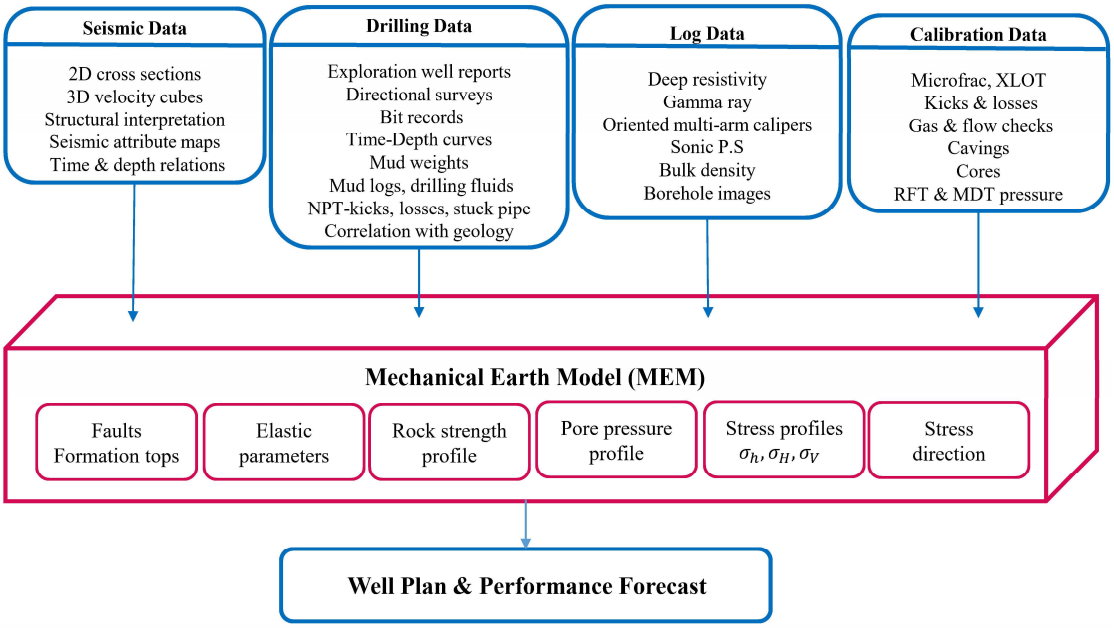

Figure 10: Required data set for constructing MEM.

Using the ideas represented in Figure **10**, the 1D MEM was constructed for Well#A, which is shown in Figures **11** and **12**. Based on the description of MEM, in Figure **11**, the elastic and strength property profiles of Well#A are shown. Track 1 shows the depth in meters. In track 2, the dynamic and static Young's modulus (GPa) are shown. The third track presents the static shear and static bulk modulus (GPa). Track 4 represents Poisson's ratio. Finally, track 5 displays the strength parameters. UCS, tensile strengths (MPa), and the friction angle (FANG) of the formations are shown in this track.

The stress profiles with the pore pressure profile (P_P), which was constructed based on the empirical relations and MDT pressure data, are shown in Figure **12**. In Figure **12a**, pore pressure was estimated by Equation (17), while Figure **12b** was plotted based on Equation (22). As can be seen in Figure **12a**, the Sighmin (σ_h) is close to the XLOT data point at a depth of 3513 (m), which was used for calibrating the estimated minimum horizontal stress. Also, the pore pressure profile was calibrated by RFT data points at different zones of the reservoir. Based on the results, the estimated minimum horizontal stress (σ_h) and pore pressure showed good matching with XLOT and RFT points. Hence, the results showed low to moderate stress anisotropy. While in the upper and lower depths, the order of the stress magnitude is SigHmax>Sighmin>SigV, changing to nearly strike-slip (SigHmax>SigV>Sighmin) regime in the depths where the SigV is larger than Sighmin (see Figure **12a**). As seen in Figure **12b**, for the most part, except in the upper and lower parts of the graph, the dominant stress regime is SigHmax>SigV>Sighmin, and also Sighmin at a depth of 3513 (m) is 78.44 that is very close to the XLOT value which is 78.67 at this depth.

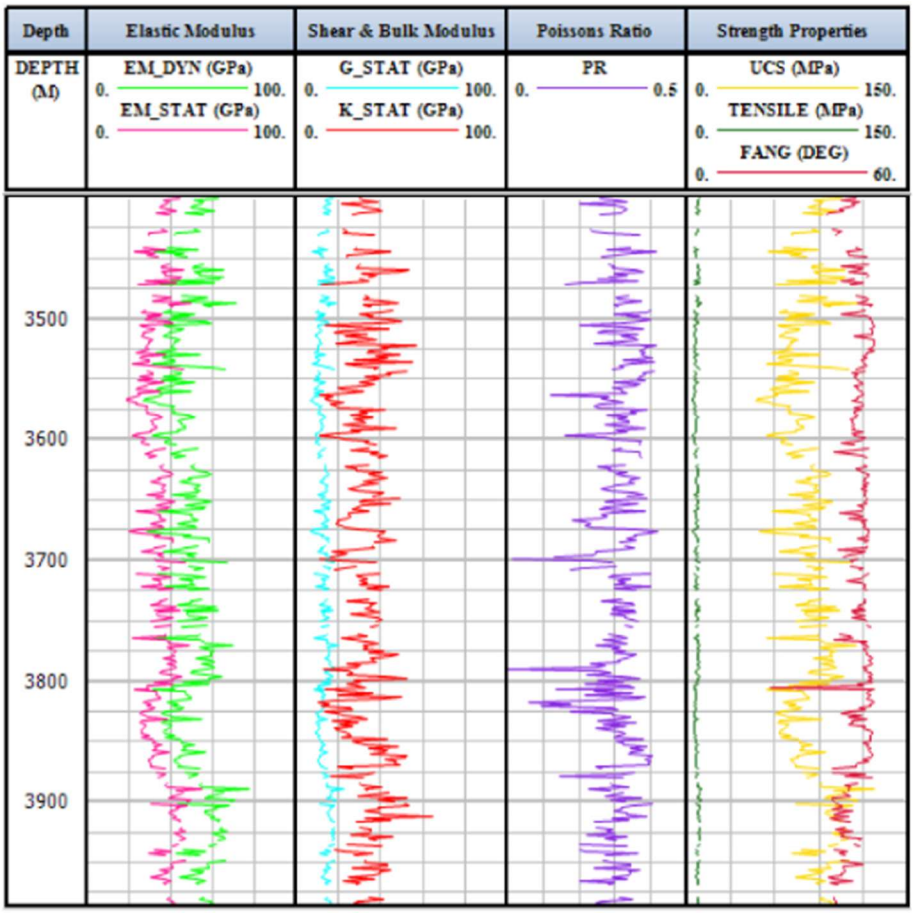

Figure 11: Elastic modulus and strength profiles estimated in Well#A.

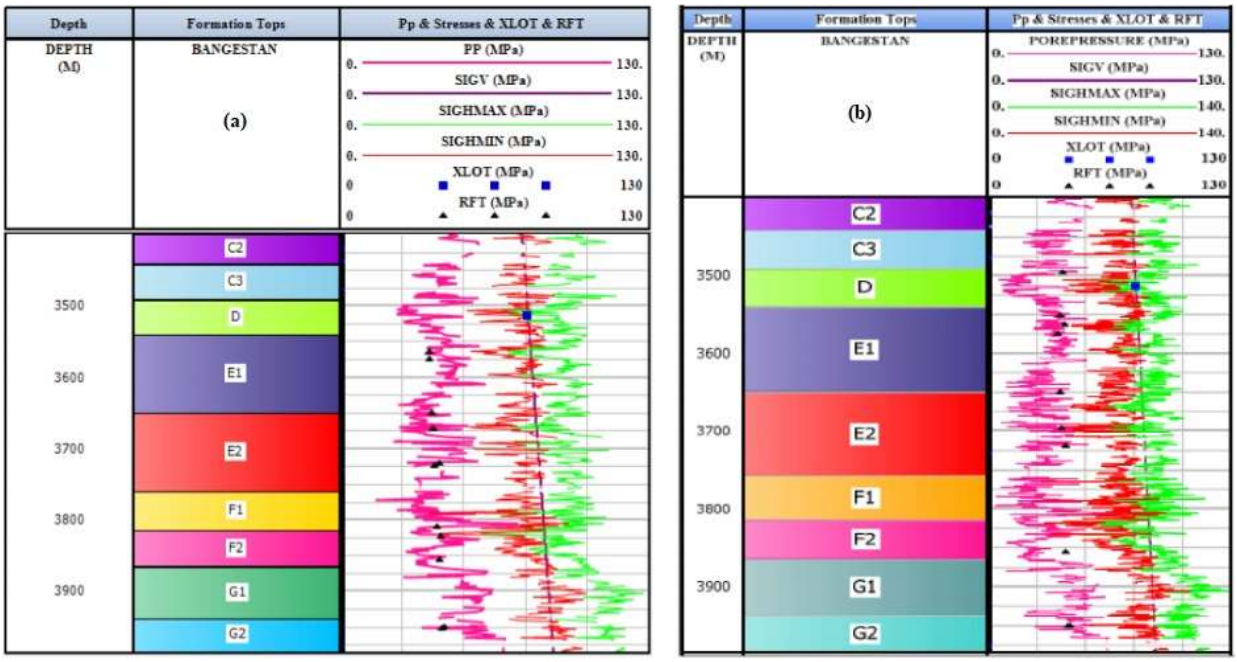

Figure 12: Pore pressure and stress profiles in Well#A based on the (a) Literature equation (b) Introduced equation.

4.3. Candidate Zone Selection for Simulating Hydraulic Fracturing

The initiation and propagation of hydraulic fracturing in carbonate reservoirs are significantly affected by the reservoir's mechanical properties [78, 79]. For instance, during hydraulic fracturing operation, the layers with high Young's modulus and low porosity would cause narrow fractures, while the layers with low Young's modulus and high porosity would yield wider fractures. Selecting suitable zones and intervals is one of the most challenging issues in hydraulic fracturing simulation/operation. Thus, for selecting the suitable zones, three main properties, including hydrocarbon volume, water saturation, and effective porosity, should be considered [80, 81]. Thus, the zones having high hydrocarbon volume, low water saturation, and high effective porosity could be the most desired zones. Furthermore, vuggy porosity and existing fractures could be good signs that the reservoir might be productive [82, 83].

Therefore, in this study and based on the drill hole results, we concluded that the vuggy porosity is the most common porosity in the studied sections, and it shows a high percentage in zones C2, E2, and G2, according to Figure **8**. Besides, the laboratory results showed the values of porosity, permeability, and water saturation for different zones in studied wells (Table **4** and Figure **13**); and based on the petrophysical reservoir properties, C2, E2, and G2 were selected as suitable reservoir zones.

Table 4: Petrophysical properties of different reservoir zones.

Zone	Porosity (%)	Permeability (mD)	Water Saturation (%)
C2	14.5	31	21
C3	8	3.9	53
D	3	5.2	67
E1	5.7	13.1	35.6
E2	10	11.7	34
F1	2.8	0.75	57.8
F2	3	12.6	56
G1	6.7	4	37
G2	9.6	5	36.6

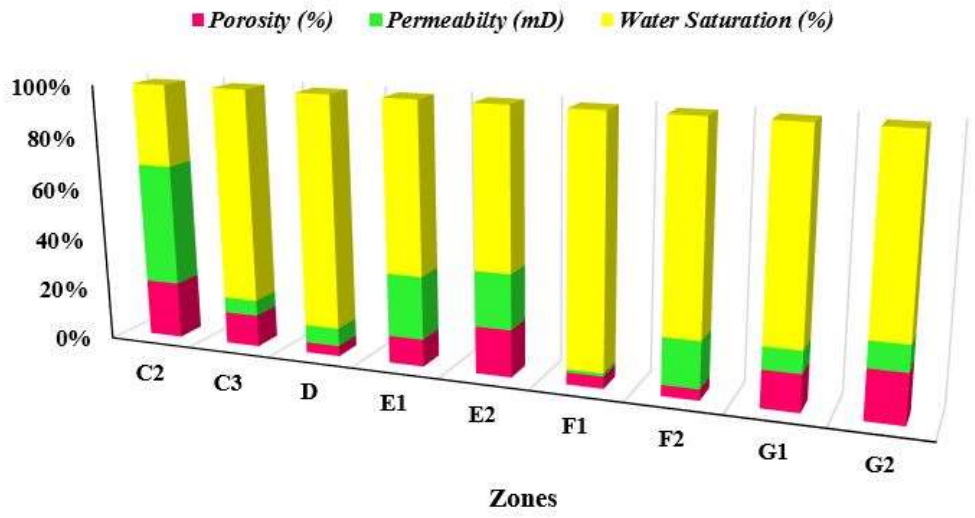

Figure 13: Distribution of petrophysical parameters in zones C2 to G2.

Finally, based on the obtained geomechanical parameters of the studied zones (Table **1** and Figures **14**, **15**, **16**) and also considering the results obtained in the two first phases of this study, zones E2 and G2 were selected as candidate zones for hydraulic fracturing operation. Based on the previous studies [84], hydraulic fractures are best if they are longer and narrower. So, in this case, the layers with higher Young's modulus and lower porosity are the best targets because they would lead to the narrow fractures for best performance. Based on our results, the E2 and G2 zones were selected for hydraulic fracturing operations.

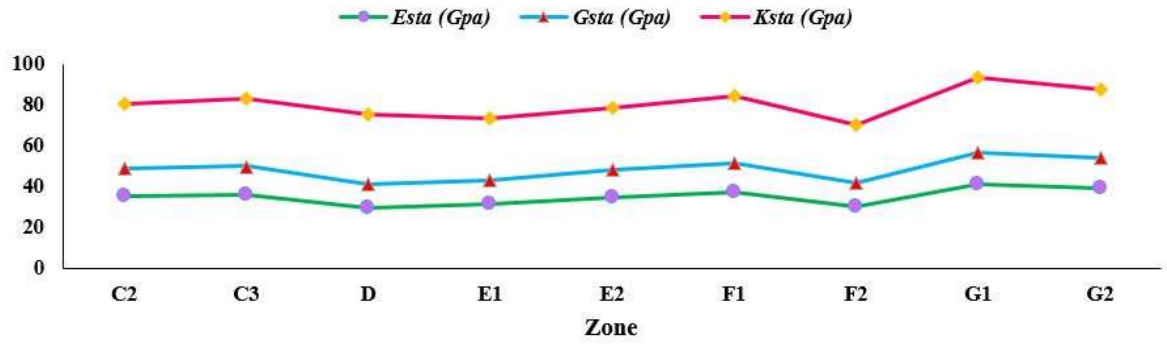

Figure 14: Static elastic parameters vs. zones in Well#A.

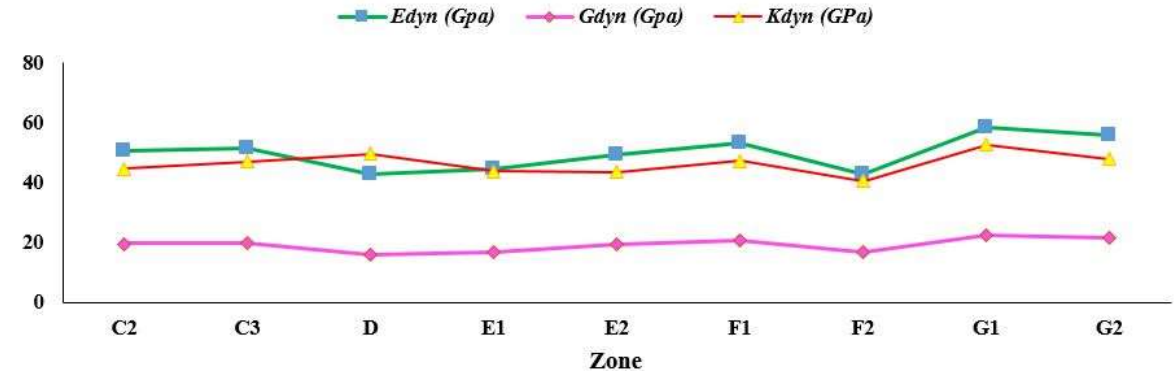

Figure 15: Dynamic elastic parameters vs. zones in Well#A.

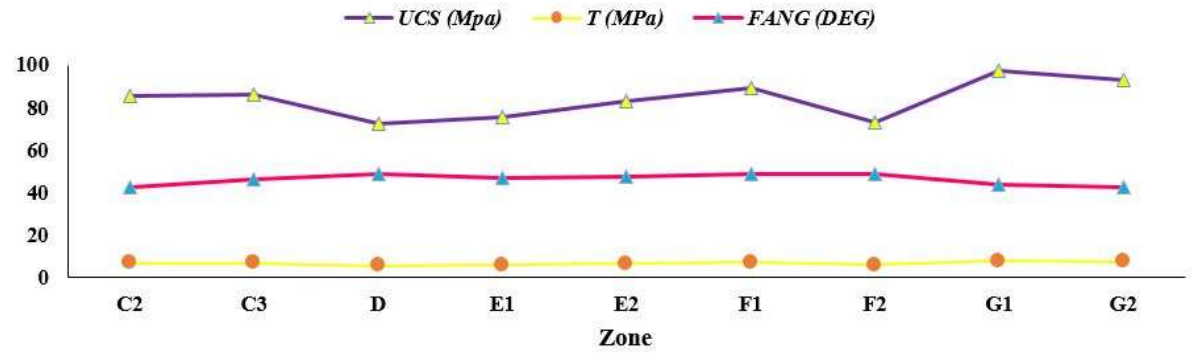

Figure 16: Strength parameters vs. zones in Well#A.

5. Conclusion and Recommendation

In order to overcome the shortcomings of previous investigations, diagenetic, petrophysical, and geomechanical data were used for selecting a hydraulic fracturing candidate zone in one of the Iranian carbonate oil reservoirs.

By developing a method of combining various available data, more comprehensive information from the reservoir will be obtained, which will offer more accuracy in designing and operating hydraulic fracturing, as well as selecting candidate zone(s).

From an innovative point of view, we can refer to the combination of three data sets, including diagenetic, petrophysical, and geomechanical data, for the first time for candidate zone selection for hydraulic fracturing operations in Iran's carbonate reservoirs. Besides, a new empirical relationship was introduced for calculating pore pressure in all zones of the studied well.

The observed changes in maximum and minimum horizontal stresses and pore pressure based on the equation presented in the literature ($DT_n = 0.000234D + 50.078$) and the new empirical equation was obtained in this study ($\mathrm{DT_n} = 0.000317\mathrm{D} + 53.08$) were as follows: 9.74 reductions in pore pressure, 0.1 increase in SigHmax, and 1.22 reduction in Sighmin.

Rock changes in each formation and depth are considered by the new equation. Therefore, it provides more acceptable results that are closer to the real in situ conditions.

Based on the study results, pore pressure calculations, and the newly introduced empirical equation for every nine zones in the studied well, and pore pressure is presented as below:

$$DT_n = \chi D + \xi$$

$$\begin{aligned}
&If\ \chi = 0.01890 \quad \& \quad \xi = -157.1 \rightarrow Zone\,C2\\
&If\ \chi = -0.00063 \quad \& \quad \xi = 61.1 \rightarrow Zone\,C3\\
&If\ \chi = -0.01207 \quad \& \quad \xi = 196 \rightarrow Zone\,D\\
&If\ \chi = -0.01997 \quad \& \quad \xi = 293.5 \rightarrow Zone\,E1\\
&If\ \chi = -0.00676 \quad \& \quad \xi = 137.3 \rightarrow Zone\,E2\\
&If\ \chi = -0.04198 \quad \& \quad \xi = -464.9 \rightarrow Zone\,F1\\
&If\ \chi = -0.12339 \quad \& \quad \xi = 1619.4 \rightarrow Zone\,F2\\
&If\ \chi = -0.02239 \quad \& \quad \xi = 340.6 \rightarrow Zone\,G1\\
&If\ \chi = -0.01507 \quad \& \quad \xi = 251.4 \rightarrow Zone\,G2
\end{aligned}$$

Based on the newly introduced equation, the dominant stress regime in the studied area is SigHmax>SigV>Sighmin, and the stress anisotropy is much less than the one obtained using the equation presented by previous researchers.

Candidate well/zone selection for the hydraulic fracturing operation would be a challenging job due to its vital role in the success or failure of the treatment. Therefore, it is a very important step.

E2 and G2 zones were chosen as the best zones for hydraulic fracture operations.

The availability of DTCO and DTSM of the reservoir improves the possibility of constructing 1D MEM with more accuracy.

6. Recommendation

In some cases that the stress regimes are not normal, hydraulic fracturing propagation and geometry are usually more complex to predict. In these cases, performing numerical simulation for investigating the hydraulic fracturing geometry is recommended.

After all, hydraulic fracturing stimulation in candidate zones is recommended for future work, but following the development of new technologies for carbonate reservoir stimulation, methods such as hybrid volume

stimulation (HVS) are proposed for tightly fractured carbonate reservoirs [85]. Based on this method, there are three main stages for reservoir stimulation which include hydraulic fracturing, large-scale acid fracturing, and proppant injection. Therefore, it is suggested that after the necessary evaluations, if the process is economical, the HVS method is performed for this area.

Acknowledgment (Funding)

This work was supported by the “Iran National Science Foundation (INSF) (No. 98011044)” and also “Research Institute of Petroleum Industry (RIPI)”.

Declarations

Elham Bakhshi carried out the research, interpreted the results, and wrote the original manuscript. Abbas Shahrabadi and Naser Golsanami guided and supervised the application of the methodology. A technical review was carried out by Naser Golsanami. Technical information was provided by Shahrzad Seyedsajadi, Xiaoqiang Liu, and Ziquan Wang.

Conflicts of Interest

The authors declare no conflict of interest.

List of Symbols

$\sigma_H, \sigma_h, \sigma_v$	Maximum and minimum horizontal stresses and vertical stress, respectively (MPa)
P_p	Pore Pressure (MPa)
E_{sta}, E_{dyn}	Static and dynamic Young’s modulus, respectively (GPa)
ν_{sta}, ν_{dyn}	Static and dynamic Poisson’s ratio, respectively
G_{sta}, G_{dyn}	Static and dynamic shear modulus, respectively (GPa)
K_{sta}, K_{dyn}	Static and dynamic bulk modulus, respectively (GPa)
V_p, V_s	Compression and shear wave velocity, respectively (m/s)
ρ	Rock density (gr/cm^3)
UCS	Unconfined compressive strength (MPa)
T	Tensile strength (MPa)
FANG	Internal friction angle (Degree)
α	Biot's coefficient
$\varepsilon_x, \varepsilon_y$	Horizontal strains
ν_{sh}	Shale volume (v/v)
GR	Gamma ray (GAPI)
Δt	Acoustic travel time (μs/ft)
DTCO	Compressional wave delay time (μs/ft)
DTSM	Shear wave delay time (μs/ft)
S_w	Water saturation (%)
RFT	Repeat formation test
LOT	Leak-off test
TVD	True vertical depth (m)

References

[1] Van Buchem F, *et al*. Regional stratigraphic architecture and reservoir types of the Oligo-Miocene deposits in the Dezful Embayment (Asmari and Pabdeh Formations) SW Iran. Geological Society, London, Special Publications, 2010; 329(1): p. 219-263. https://doi.org/10.1144/SP329.10

[2] Bize-Forest N*, et al.* Carbonate reservoir rock typing and the link between routine core analysis and special core analysis. in International symposium of the society of core analysts. 2014.

[3] Xu C, Heidari Z, Torres-Verdin C. Rock classification in carbonate reservoirs based on static and dynamic petrophysical properties estimated from conventional well logs. in SPE Annual Technical Conference and Exhibition. 2012; Society of Petroleum Engineers. https://doi.org/10.2118/159991-MS

[4] Ali SA, *et al*. Diagenesis and reservoir quality. Oilfield Review, 2010; 22(2): p. 14-27.

[5] Qiang L, *et al*. Petrophysical characteristics and logging evaluation of asphaltene carbonate reservoirs: A case study of the Cambrian Longwangmiao Formation in Anyue gas field, Sichuan Basin, SW China. Petroleum Exploration and Development, 2017; 44(6): p. 941-947. https://doi.org/10.1016/S1876-3804(17)30106-4

[6] Kumar M, *et al*. Petrophysical evaluation of well log data and rock physics modeling for characterization of Eocene reservoir in Chandmari oil field of Assam-Arakan basin, India. Journal of Petroleum Exploration and Production Technology, 2018; 8(2): p. 323-340. https://doi.org/10.1007/s13202-017-0373-8

[7] Jia Y, *et al*. Laboratory geomechanical and petrophysical characterization of Longmaxi shale properties in Lower Silurian Formation, China. Marine and Petroleum Geology, 2021; 124: p. 104800. https://doi.org/10.1016/j.marpetgeo.2020.104800

[8] Siddiqui N.A, *et al*. Sedimentological characterization, petrophysical properties and reservoir quality assessment of the onshore Sandakan Formation, Borneo. Journal of Petroleum Science and Engineering, 2020; 186: p. 106771. https://doi.org/10.1016/j.petrol.2019.106771

[9] Yin S, *et al*. Experimental investigation of the petrophysical properties, minerals, elements and pore structures in tight sandstones. Journal of Natural Gas Science and Engineering, 2020; 76: p. 103189. https://doi.org/10.1016/j.jngse.2020.103189

[10] Golsanami N, *et al*. NMR-based study of the pore types' contribution to the elastic response of the reservoir rock. Energies, 2021; 14(5): p. 1513. https://doi.org/10.3390/en14051513

[11] Golsanami N, *et al*. Fractal Properties of Various Clay Minerals Obtained from SEM Images. Geofluids, 2021; 2021. https://doi.org/10.1155/2021/5516444

[12] Dong H, *et al*. A method to construct high-precision complex pore digital rock. Journal of Geophysics and Engineering, 2018; 15(6): p. 2695-2703. https://doi.org/10.1088/1742-2140/aae04e

[13] Dong X, *et al*. How N2 injection improves the hydrocarbon recovery of CO2 HnP: An NMR study on the fluid displacement mechanisms. Fuel, 2020; 278: p. 118286. https://doi.org/10.1016/j.fuel.2020.118286

[14] Gaddipati M*, et al.* An Integrated Reservoir Modeling Case Study to Simulate Multi-Stage Hydraulically Fractured Horizontal Wells, based on Seismic, Petrophysical and Geological data for Pinedale Tight Gas Fluvial Reservoir. in Unconventional Resources Technology Conference, 20-22 July 2020; 2020. Unconventional Resources Technology Conference (URTeC). https://doi.org/10.15530/urtec-2020-2582

[15] Iqbal O, Ahmad M, Abd Kadir A. Effective evaluation of shale gas reservoirs by means of an integrated approach to petrophysics and geomechanics for the optimization of hydraulic fracturing: A case study of the Permian Roseneath and Murteree Shale Gas reservoirs, Cooper Basin, Australia. Journal of Natural Gas Science and Engineering, 2018; 58: p. 34-58. https://doi.org/10.1016/j.jngse.2018.07.017

[16] Richards G*, et al.* Hydraulic Fracturing in Heterogenous Reservoirs; Modelling at Petrophysical vs. Geomechanical Resolution. in 54th US Rock Mechanics/Geomechanics Symposium. 2020; American Rock Mechanics Association.

[17] Shalaby MR. Petrophysical characteristics and hydraulic flow units of reservoir rocks: Case study from the Khatatba Formation, Qasr field, North Western Desert, Egypt. Journal of Petroleum Science and Engineering, 2021; 198: p. 108143. https://doi.org/10.1016/j.petrol.2020.108143

[18] Bakhshi E, Golsanami N, Chen L. Numerical modeling and lattice method for characterizing hydraulic fracture propagation: a review of the numerical, experimental, and field studies. Archives of Computational Methods in Engineering, 2020: p. 1-32.

[19] Bakhshi E, *et al*. Lattice numerical simulations of hydraulic fractures interacting with oblique natural interfaces. International Journal of Mining and Geo-Engineering, 2019; 53(1): p. 83-89.

[20] Bakhshi E, *et al*. Lattice numerical simulations of lab-scale hydraulic fracture and natural interface interaction. Rock Mechanics and Rock Engineering, 2019; 52(5): p. 1315-1337. https://doi.org/10.1007/s00603-018-1671-2

[21] Golsanami N, *et al*. Relationships between the geomechanical parameters and Archie's coefficients of fractured carbonate reservoirs: a new insight. Energy Sources, Part A: Recovery, Utilization, and Environmental Effects, 2020: p. 1-25. https://doi.org/10.1080/15567036.2020.1849463

[22] Liu X, *et al*. Numerical simulation of non-planar fracture propagation in multi-cluster fracturing with natural fractures based on Lattice methods. Engineering Fracture Mechanics, 2019; 220: p. 106625. https://doi.org/10.1016/j.engfracmech.2019.106625

[23] Bakhshi E, *et al*. Hydraulic fracture propagation: analytical solutions versus Lattice simulations. Journal of Mining and Environment, 2019; 10(2): p. 451-464.

[24] Eltom HA, *et al*. Effect of bioturbation on petrophysical properties: Insights from geostatistical and flow simulation modeling. Marine and Petroleum Geology, 2019; 104: p. 259-269. https://doi.org/10.1016/j.marpetgeo.2019.03.019

[25] Okon AN, Adewole SE, Uguma EM. Artificial neural network model for reservoir petrophysical properties: porosity, permeability and water saturation prediction. Modeling Earth Systems and Environment, 2020: p. 1-18. https://doi.org/10.1007/s40808-020-01012-4

[26] Higgins-Borchardt S, Sitchler J, Bratton T. Geomechanics for unconventional reservoirs, in Unconventional Oil and Gas Resources Handbook. 2016, Elsevier. p. 199-213. https://doi.org/10.1016/B978-0-12-802238-2.00007-9

[27] Wendt AS, *et al*. Three-dimensional mechanical earth modeling. 2013, Google Patents.

[28] Fattahpour V*, et al.* Building a mechanical earth model: a reservoir in Southwest Iran. in 46th US Rock Mechanics/Geomechanics Symposium. 2012; American Rock Mechanics Association.

[29] Algarhy A, Dubey A. Uncertainty Reduction in Constructing the Mechanical Earth Model Using Artificial Neural Network: Case Study from Egypt's Western Desert. in 53rd US Rock Mechanics/Geomechanics Symposium. 2019; American Rock Mechanics Association.

[30] Cuervo S, Adachi J, Lombardo E. Integration of 1D and 3D Mechanical Earth Models in Oil Shale Plays. an Example From the Vaca Muerta Formation (Argentina). in 52nd US Rock Mechanics/Geomechanics Symposium. 2018; American Rock Mechanics Association.

[31] JU W, *et al*. Stress Distribution in the Upper Shihezi Formation from 1D Mechanical Earth Model and 3D Heterogeneous Geomechanical Model, Linxing region, Eastern Ordos Basin, Central China. Acta Geologica Sinica-English Edition.

[32] Li Q*, et al.* Geomechanical Characterization and Modeling in the Montney for Hydraulic Fracturing Optimization. in SPE Canada Unconventional Resources Conference. 2020; Society of Petroleum Engineers. https://doi.org/10.2118/199978-MS

[33] Shahbazi K, Abdideh M, Hadipoor M. Modelling hydraulic fracturing process in one of the Iranian southwest oil reservoirs. Applied Earth Science, 2017; 126(3): p. 108-117. https://doi.org/10.1080/03717453.2017.1322395

[34] Sirat M, Ahmed M, Zhang X. Predicting hydraulic fracturing in a carbonate gas reservoir in Abu Dhabi using 1D mechanical earth model: uncertainty and constraints. in SPE Middle East Unconventional Resources Conference and Exhibition. 2015; Society of Petroleum Engineers. https://doi.org/10.2118/172942-MS

[35] Keshavarzi R, Jalili S. Building a mechanical earth model and its application in a geomechanical analysis of hydraulic fracture behaviour in naturally fractured reservoirs. European journal of environmental and civil engineering, 2014; 18(3): p. 336-357. https://doi.org/10.1080/19648189.2013.856035

[36] Afsari M*, et al.* Mechanical Earth Model (MEM): an effective tool for borehole stability analysis and managed pressure drilling (Case Study). in SPE Middle East Oil and Gas Show and Conference. 2009; Society of Petroleum Engineers. https://doi.org/10.2118/118780-MS

[37] Afsari M*, et al.* Using drilling and logging data for developing 1d mechanical earth model for a mature oil field to predict and mitigate wellbore stability challenges. in International Oil and Gas Conference and Exhibition in China. 2010; Society of Petroleum Engineers. https://doi.org/10.2118/132187-MS

[38] Adegbamigbe T, Olamigoke O, Lawal K. Application of a 1-D Mechanical Earth Model for Wellbore Stability Analysis in a Shallow-Water Field, Niger Delta. in SPE Nigeria Annual International Conference and Exhibition. 2020; Society of Petroleum Engineers. https://doi.org/10.2118/203632-MS

[39] Bakhshi E, Shahrabadi A, Golsanami N. Cavings' role in representing the type of wellbore failures in fractured reservoirs, in Fifth International Conference on Oil, Gas, Petrochemical & HSE. 2021: Hamedan, Iran.

[40] Kidambi T, Kumar GS. Mechanical earth modeling for a vertical well drilled in a naturally fractured tight carbonate gas reservoir in the Persian Gulf. Journal of Petroleum Science and Engineering, 2016; 141: p. 38-51. https://doi.org/10.1016/j.petrol.2016.01.003

[41] Zain-Ul-Abedin M, Henk A. Building 1D and 3D Mechanical Earth Models for Underground Gas Storage-A Case Study from the Molasse Basin, Southern Germany. Energies, 2020; 13(21): p. 5722. https://doi.org/10.3390/en13215722

[42] Heydarabadi FR*, et al.* Criteria for selecting a candidate well for hydraulic fracturing. in Nigeria Annual International Conference and Exhibition. 2010; Society of Petroleum Engineers. https://doi.org/10.2118/136988-MS

[43] Zoveidavianpoor M, Samsuri A, Shadizadeh SR. Development of a fuzzy system model for candidate-well selection for hydraulic fracturing in a carbonate reservoir. in SPE Oil and Gas India Conference and Exhibition. 2012; OnePetro. https://doi.org/10.2118/153200-MS

[44] Burenina IV, *et al*. Improving methodological approach to measures planning for hydraulic fracturing in oil fields. Записки Горного института, 2019; 237. https://doi.org/10.31897/pmi.2019.3.343

[45] Hashemi A, Shadizadeh SR, Zoveidavianpoor M. A local computerized multi-screening of vast amount of data to select hydraulic fracturing candidates in Iranian carbonate oil fields. International Journal of Computer Applications, 2012; 975: p. 8887. https://doi.org/10.5120/4842-7106

[46] Zoveidavianpoor M, Samsuri A, Shadizadeh SR. Fuzzy logic in candidate-well selection for hydraulic fracturing in oil and gas wells: A critical review. International Journal of Physical Sciences, 2012; 7(26): p. 4049-4060. https://doi.org/10.5897/IJPS12.042

[47] Hashemi A, Shadizadeh SR, Zoveidavianpoor M. Selection of hydraulic fracturing candidates in iranian carbonate oil fields: a local computerised screening of zone and well data. in International Petroleum Technology Conference. 2013; OnePetro. https://doi.org/10.2523/IPTC-17192-MS

[48] Esrafili-Dizaji B, Rahimpour-Bonab H. CARBONATE RESERVOIR ROCKS AT GIANT OIL AND GAS FIELDS IN SW IRAN AND THE ADJACENT OFFSHORE: A REVIEW OF STRATIGRAPHIC OCCURRENCE AND PORO-PERM CHARACTERISTICS. Journal of Petroleum Geology, 2019; 42(4): p. 343-370. https://doi.org/10.1111/jpg.12741

[49] Rahimpour-Bonab H, *et al*. Palaeo-exposure surfaces in Cenomanian-santonian carbonate reservoirs in the Dezful embayment, SW Iran. Journal of Petroleum Geology, 2013; 36(4): p. 335-362. https://doi.org/10.1111/jpg.12560

[50] Esrafili-Dizaji B, *et al*. Characterization of rudist-dominated units as potential reservoirs in the middle Cretaceous Sarvak Formation, SW Iran. Facies, 2015; 61(3): p. 14. https://doi.org/10.1007/s10347-015-0442-8

[51] Nasseri A, Mohammadzadeh MJ, HashemTabatabaee S. Evaluating Bangestan reservoirs and targeting productive zones in Dezful embayment of Iran. Journal of Geophysics and Engineering, 2016; 13(6): p. 994-1001. https://doi.org/10.1088/1742-2132/13/6/994

[52] Bordenave M, Hegre J. Current distribution of oil and gas fields in the Zagros Fold Belt of Iran and contiguous offshore as the result of the petroleum systems. Geological Society, London, Special Publications, 2010; 330(1): p. 291-353. https://doi.org/10.1144/SP330.14

[53] Choquette PW, Pray LC. Geologic nomenclature and classification of porosity in sedimentary carbonates. AAPG bulletin, 1970; 54(2): p. 207-250. https://doi.org/10.1306/5D25C98B-16C1-11D7-8645000102C1865D

[54] James NP, Choquette PW. Diagenesis 9. Limestones-the meteoric diagenetic environment. Geoscience Canada, 1984.

[55] Heydari E, Moore CH. Burial diagenesis and thermochemical sulfate reduction, Smackover Formation, southeastern Mississippi salt basin. Geology, 1989; 17(12): p. 1080-1084. https://doi.org/10.1130/0091-7613(1989)017<1080:BDATSR>2.3.CO;2

[56] Flugel E. Microfacies of carbonate rocks: analysis, interpretation and application. 2004: Springer Science & Business Media. https://doi.org/10.1007/978-3-662-08726-8

[57] Tucker M. Geological background to carbonate sedimentation. Carbonate sedimentology, 1990; https://doi.org/10.1002/9781444314175

[58] Tucker M. Sedimentary Petrology-An Introduction to the Origin of Sedimentary Rocks. − Blackwell. Scientific publication, London, 2001.

[59] Whitaker FF, Xiao Y. Reactive transport modeling of early burial dolomitization of carbonate platforms by geothermal convection. AAPG bulletin, 2010; 94(6): p. 889-917. https://doi.org/10.1306/12090909075

[60] Moore CH. Carbonate diagenesis and porosity. 1989: Elsevier.

[61] Bathurst RG. Carbonate sediments and their diagenesis. 1972: Elsevier.

[62] Moore CH, Wade WJ. The nature and classification of carbonate porosity, in Developments in sedimentology. 2013, Elsevier. p. 51-65. https://doi.org/10.1016/B978-0-444-53831-4.00004-5

[63] Esteban M, Taberner C. Secondary porosity development during late burial in carbonate reservoirs as a result of mixing and/or cooling of brines. Journal of Geochemical Exploration, 2003; 78: p. 355-359. https://doi.org/10.1016/S0375-6742(03)00111-0

[64] Narongsirikul S, Mondol NH, Jahren J. Acoustic and petrophysical properties of mechanically compacted overconsolidated sands: part 1-experimental results. Geophysical Prospecting, 2019; 67(4): p. 804-824. https://doi.org/10.1111/1365-2478.12744

[65] Horsrud P. Estimating mechanical properties of shale from empirical correlations. SPE Drilling & Completion, 2001; 16(02): p. 68-73. https://doi.org/10.2118/56017-PA

[66] Archer S, Rasouli V. A log based analysis to estimate mechanical properties and in-situ stresses in a shale gas well in North Perth Basin. Petroleum and Mineral Resources, 2012; 21: p. 122-135. https://doi.org/10.2495/PMR120151

[67] Davies DH, Davies O, Horsfall OI. Determination of Geomechanical Properties of a typical Niger Delta Reservoir Rock Using Geophysical Well Logs. Davies, Dein Honour, 2019: p. 222-233.

[68] Golsanami N, *et al*. Relationships between the geomechanical parameters and Archie's coefficients of fractured carbonate reservoirs: A new insight. Energy Sources, Part A: Recovery, Utilization, and Environmental Effects Journal, 2020: p. 1-24. https://doi.org/10.1080/15567036.2020.1849463

[69] Al-Qahtani MY, Zillur R. A mathematical algorithm for modeling geomechanical rock properties of the Khuff and Pre-Khuff reservoirs in Ghawar field. in SPE Middle East Oil Show. 2001; Society of Petroleum Engineers. https://doi.org/10.2118/68194-MS

[70] Fjar E, *et al*. Petroleum related rock mechanics. 2008: Elsevier.

[71] Eaton BA. Graphical method predicts geopressures worldwide. World Oil;(United States), 1976; 183(1).

[72] Khan N, Hanif M. Abnormal Formation Pressure in the Sulaiman Province, Pakistan: An Insight into Factor Affecting Reservoirs in a Compressional Strike-Slip Region. Arabian Journal for Science and Engineering, 2020; 45(6): p. 4853-4870. https://doi.org/10.1007/s13369-020-04419-4

[73] Tingay MR, *et al*. Origin of overpressure and pore-pressure prediction in the Baram province, Brunei. Aapg Bulletin, 2009; 93(1): p. 51-74. https://doi.org/10.1306/08080808016

[74] Mazzullo S. Overview of porosity evolution in carbonate reservoirs. Kansas Geological Society Bulletin, 2004; 79(1-2): p. 1-19.

[75] Tingay MR, *et al*. Present-day stress and neotectonics of Brunei: Implications for petroleum exploration and production. AAPG bulletin, 2009; 93(1): p. 75-100. https://doi.org/10.1306/08080808031

[76] Sen S, Kundan A, Kumar M. Post-drill analysis of pore pressure and fracture gradient from well logs and drilling events-An integrated case study of a high pressure exploratory well from Panna East, Mumbai Offshore Basin, India. in Pore pressure and geomechanics from exploration to abandonment, AAPG geosciences technology workshop, Perth, Australia, June. 2018.

[77] Ganguli SS, Sen S. Investigation of present-day in-situ stresses and pore pressure in the south Cambay Basin, western India: Implications for drilling, reservoir development and fault reactivation. Marine and Petroleum Geology, 2020; 118: p. 104422. https://doi.org/10.1016/j.marpetgeo.2020.104422

[78] Josh M, *et al*. Laboratory characterisation of shale properties. Journal of Petroleum Science and Engineering, 2012; 88: p. 107-124. https://doi.org/10.1016/j.petrol.2012.01.023

[79] Li J, *et al*. Quantitative evaluation on the elastic property of oil-bearing mudstone/shale from a Chinese continental basin. Energy Exploration & Exploitation, 2015; 33(6): p. 851-868. https://doi.org/10.1260/0144-5987.33.6.851

[80] Darvish H, *et al*. Geo-mechanical modeling and selection of suitable layer for hydraulic fracturing operation in an oil reservoir (south west of Iran). Journal of African Earth Sciences, 2015; 111: p. 409-420. https://doi.org/10.1016/j.jafrearsci.2015.08.001

[81] Perumalla S*, et al.* Role of Geomechanics in appraisal of a deep tight gas reservoir: A case history from the Amin formation in the Sultanate of Oman. in SPE Middle East Unconventional Gas Conference and Exhibition. 2011; OnePetro. https://doi.org/10.2118/142788-MS

[82] Xiao Y, *et al*. Dynamic and static combination method for fracture-vug unit division of fractured-vuggy reservoirs. Arabian Journal for Science and Engineering, 2018; 43(5): p. 2633-2640. https://doi.org/10.1007/s13369-017-2976-2

[83] Baniasadi H, Rashidi F. A triple-porosity radial composite model for two phase well test analysis of volatile oil in fractured-vuggy reservoirs. Scientia Iranica, 2021.

[84] Donaldson E, Alam W, Begum N. Hydraulic fracturing explained. Hydraulic Fracturing Explained: Evaluation, Implementation, and Challenges, 2013: p. 1-22. https://doi.org/10.1016/B978-1-933762-40-1.50010-6

[85] Guo J, *et al*. Comprehensive study of fracture flow characteristic and feasibility of hybrid volume stimulation technique in tight fractured carbonate gas reservoir. Journal of Petroleum Science and Engineering, 2019; 174: p. 362-373. https://doi.org/10.1016/j.petrol.2018.11.006